Journal of Intelligent & Robotic Systems (2024) 110:137
https://doi.org/10.1007/s10846-024-02164-6

REGULAR PAPER

Introduction of a Framework for the Integration of a Kinematic Robot Arm Model in an Artificial Neural Network - Extended Kalman Filter Approach

Sabine Horvath[1] · **Hans Neuner**[1]

Received: 31 March 2024 / Accepted: 20 August 2024

Abstract
The aim of this paper is to introduce a model in which systematic effects can be assigned according to their origin or mode of action. The approach intends to improve the positional accuracy of a robot arm. We show the impact of unaccounted model biases on estimated parameters when applying sequential approaches and conclude the necessity of jointly determining all influencing variables. Therefore, we propose a simultaneous estimation of transformation parameters, robot's kinematic parameters and non-geometric parameters modelled by an artificial neural network (ANN) in further consequence. Thus, the main contribution of this paper is a new approach of the simultaneous estimation of the geometric and non-geometric components of a robot arm model. The integration of the geometric model (transformations, kinematic robot model) with the non-geometric one (ANN) is realised in the extended Kalman filter. The functionality of the algorithm has been proven on simulated data. The adaptive behaviour of machine learning approaches is made possible by an additional iteration of the ANN. The initialisation of the ANN parameters must not deviate from the nominal parameters by more than 10% so that the ANN can learn the non-geometric part. In this setup, the robot arm position corrections are reduced by 32.5%. A final sensitivity analysis proves the estimability of most kinematic parameters in the course of a future adaptive extension of the approach.

Keywords Artificial neural networks · Extended Kalman filter · Robot arm · Calibration

1 Introduction and Related Work

An increase in the pose accuracy of robot arms leads to an increase in production in many areas e.g. the automotive or aerospace industries as well as a broadening of the areas of applications i.e. additive manufacturing. This applies in particular to welding [1] and gripping [2] processes. Pose accuracy is also important in feedback control of robot arms [3] when employing them for i.e. assistance activities [4]. The aim of this work is to improve the positioning accuracy of robot arms by feedforward control [5]. This is to be achieved by combining complementary methods. The following terms are important in the course of this article and their formulation should contribute to a better understanding. In general, a distinction is made between parametric and non-parametric methods [6]. "Parametric models are described by a few parameters, which are adequate to characterize the accuracy of a model" [6, p. 321]. These include the classical approaches of kinematic and dynamic calibration. In contrast, non-parametric models are required when the systems properties are very complicated [6]. These systems can be modelled using ARMA models or special variants thereof [7], but machine learning (ML) methods [8] can also be used. In particular, we distinguish between geometric and non-geometric methods, with kinematic robot calibration as a purely geometric method belonging to the former and dynamic robot calibration taking forces into account belonging to the latter. For geometric approaches or kinematic robot arm calibration, we refer to [9] for an advanced procedure. A representative for non-geometric approaches or dynamic robot arm calibration is Aoyagi et al. [10]. In general, the focus of this article is the combination of parametric and non-parametric methods.

✉ Sabine Horvath
sabine.horvath@tuwien.ac.at

Hans Neuner
hans.neuner@tuwien.ac.at

[1] Department of Geodesy and Geoinformation, TU Wien, Wiedner Hauptstrasse 8-10, Vienna A-1040, Austria

Published online: 21 September 2024

Scientists from various disciplines are working on the topic of combining parametric methods with machine learning approaches. In [11] and [12] an overview of various combinations of parametric and non-parametric approaches in general is given. Whereas, [13] and [14] present combinations of machine learning with state estimation.

Various combinations of deep learning (non-parametric approach) and physical process models (parametric approach) are summarised in [11] and named as hybrid models. We will follow this determination in this paper. They analyse the linkages between physical models and machine learning that have been implemented to date and figured out five different general approaches. The authors conclude that data-driven approaches shall strongly complement and enrich physical modelling in their field of 'earth system sciences'. The thereby reached aim of hybrid modelling is to get 'interpretable structures and to be fully data-adaptive where theory is weak' [11]. Schlezinger et al. distinguish between model-aided networks and DNN-aided-networks [12]. In the first case, the ANN architecture imitates the operation of physical methods. In the second case, the ANN is integrated into physical methods. Jin et al. focus on data-driven state estimation - combinations of state estimation (parametric approach) and machine learning (non-parametric approach) [13]. They distinguish between three different approaches: model-observation mismatch approaches, replacing parts of the state estimation by ML (noise, transition and measurement matrix) and to directly estimate the state by ML. They conclude that these fields are worthy of attention and in depth understanding of these models is necessary. Bai et al. summarise the developments of the Kalman filter driven by machine learning [14]. They distinguish between internal and external approaches to integrate ML with Kalman filter (KF). One external combination they mention, can be found in [15]. Internal combinations, where the NN participates in the iterative process, are rather rare. An interesting area of research they point to is the accurate state estimation of robots, which conforms to the use-case of this paper.

Individual literature sources that deal with combinations of parametric and non-parametric approaches are discussed below. Stubberud et al. show one of the first combinations of an extended Kalman filter (EKF) with an ANN with their neuro-observer [16]. They integrate both the ANN itself and the ANN parameters into the state. One EKF is used for state estimation and a second EKF for ANN training. By coupling these two with an EKF, a simultaneous state estimation and ANN training is achieved. Haykin summarises various combination variants of Kalman filtering and ANN [17]. Mainly dual EKF-methods have been introduced, meaning that separate filters are connected. Abeel et al. automatically learn the noise parameters of a Kalman filter [18]. Xu and Niu [19] follow a similar approach as [18] and reach better results than [18]. Daw et al. develop a physics-guided NN, considering physical knowledge in the ANN, for modelling lake temperature [20]. They use simulation results from a physical model as inputs to an ANN and incorporate the physical inconsistency into the loss-function. This allows them to achieve better results than with baseline ML approaches. They also build a hybrid physics-data residual model, where the ANN estimates the residual error as function of the standard inputs and the physical model output and sums it with the physical model output. This enables a further reduction in the average error. The authors recognise the need for a tightly coupled combination of ANN and physical models. Willis and Stosch model structure and parameter identification for hybrid models [21]. Their focus is on the model selection of such hybrid models, especially for linear ML approaches. Fan et al. combine an ANN with ensemble KF to emulate dynamic models [22]. Their approach consists of two stages: First, they train their surrogate model, which adds to the original physical model and together they build the hybrid model. In the next step this built hybrid model is used in the ensemble KF. Hence, the ANN enters into the system equation of the KF. The effectiveness of the proposed method needs to be verified. Revach et al. specify the noise statistics and the partially known or approximated physical model as the main difficulty in the filtering approach [23]. Therefore, they replace the Kalman gain computation by a recurrent neural network in their so called 'KalmanNet'.

There is a demand for hybrid methods, combining ANN and physical models in a direct way [20]. It is assumed that not only the performance and generalisation capability, but also the consistency and credibility of hybrid methods will be improved. This may also have a positive impact on the sample complexity of ML tasks [11]. A deeper understanding of these models is needed [13] and accurate state estimation of robots is seen as a potential application area [14].

In the calibration of robot arms, Aoyagi et al. were one of the first to use ANNs to improve kinematic calibration [10]. They model joint angle deviations as a function of residual position errors. They compare the parametric modelling of the non-geometric errors of gear transmission and joint compliance with the non-parametric modelling of these errors by the ANN. The results show that the ANN reduces the average error much stronger than the parametric approaches. Nguyen et al. use the EKF instead of the standard kinematic calibration method by least squares [15]. The residual position errors are also described by an ANN, but this models the position error as a function of the joint angles. The non-geometric modelling reduces the geometric model error by about the half. The effect is less pronounced than in [10]. Zhao et al. [24] follow the approach of [15]. They increased the number of measured poses and used a deep neural network (DNN). A better result is achieved with DNNs than with shallow ANNs [15]. However, the contribution of the DNN in relation to the parametric modelling by the EKF cannot be evaluated, as the

result was not presented split up into the two parts. Gadringer et al. [25] build on the contribution by [24] - they extend the measurement system for position and orientation determination. They show that the greatest improvement is achieved by the ANN. Almost similar results are achieved by the ANN when kinematic calibration is applied or not. Selingue et al. [26] use the hybrid robot calibration model as suggested by [15] and [24] and focus on the reduction of robot positioning errors under varying payload. They derive methods to transfer a previously estimated ANN to other payloads and to interpolate between payloads by interpolating their derived ANN parameters. The literature shows that modelling non-geometric errors with ML approaches leads to lower model errors ([10] and [25]).

In ref. [27], we developed a position correction model (PCM) by an ANN. The position correction is the difference between the transformed measured robot arm position and the actual robot position. In comparison to the previously mentioned literature, no kinematic calibration was carried out. The ANN describes the robot position correction as a function of the joint angles. Different to [15], ANN and EKF build one model; EKF is mainly serving as an optimisation method. A preceding step is the determination of the transformation between the robot arm and the measurement system and the lever arm of the robot flange and the measurement point, in order to compute position corrections. Therefore an integrated determination of both parameter groups has been developed [27]. Other approaches for a simultaneous robot-world-hand-eye calibration can be found in [28] for vision-based robot control. The shortcomings of the PCM (discussed in Section 2.2.2) leads to the simultaneous estimation of the kinematic calibration (geometric effects) and the ANN, which models the non-geometric effects of the robot arm (see Section 2.3.2).

Our literature research to date has not shown any transfer of the approaches combining parametric and non-parametric methods described above to the calibration of robot arms. We present an approach that integrates a non-parametric method into the EKF. The geometric model of the robot arm is located in the system description of the EKF. The ANN, describing the non-geometrical part, is integrated in the observation equation.

The proposed integrated approach can be categorised as an "internal" approach [14], meaning that the ANN participates in the iterative process; as a "DNN-assisted inference" [12] meaning that the DNN (ANN) is integrated into a physical model; or as a mixture of a "hybrid model" (which replaces a "physical" submodel with ML) and a model-observation mismatch approach, where the difference between the physical model output and the observations is modelled by an ANN [11]. In ref. [22], the ANN is estimated in a first step. In a second step, it is incorporated into the system equation of an ensemble KF together with the physical model. This temporal sequence distinguishes it from our approach.

The main contributions of this paper are:

- Showing the impact of unaccounted model biases on estimated parameters and the necessity of jointly determining all influencing parameters
- Simultaneous estimation of geometric and non-geometric components of a robot arm system by integrating the kinematic robot arm model in an ANN-EKF approach
- Introducing the framework for the simultaneous estimation and proving the functionality on simulated data
- Achieving the adaptive behaviour of ML approaches by an additional iteration of the ANN

The article is structured as follows: Methods and data (Sec. 2) covers the basics of integrating parametric and non-parametric methods. We start with the fundamentals of the robot arm and the methods used (Sec. 2.1). In the position correction model (Sec. 2.2), the simulated data is presented and the necessity of integrating parametric and non-parametric methods is elaborated. In addition, the framework for the integration of the kinematic model into the ANN-EKF approach is presented in Section 2.3. Section 3 demonstrates the functionality and evaluates the performance of the integrated approach. The adaptivity of the ANN in simultaneous estimation is addressed in Section 3.2, the estimability of the kinematic parameters is demonstrated in a sensitivity analysis (Sec. 3.3). The limitations of the developed approach and the next steps that still need to be taken are discussed in Section 4. The article concludes with a summary in Section 5.

2 Methods and data

The basics, the arguments and the framework for the integration of geometric and non-geometric robot arm models is the content of this section. The first part deals with the object and the basics of the methods used (Sec. 2.1). Section 2.2 presents the simulated data and the position correction model, which is the starting point for all further developments. The shortcomings of the PCM (Sec. 2.2.2) and other modelling approaches (Sec. 2.2.3) then form the basis for the simultaneous estimation of the geometric and non-geometric components in the ANN-EKF approach (Sec. 2.3). The basic concepts are presented first (Sec. 2.3.1) and the detailed elaboration of the integration takes place in Section 2.3.2.

2.1 Fundamentals

This section contains an introduction to the robot arm system. The methodological fundamentals are presented - on the one hand, the ANN and, on the other hand, the estimation of an ANN in the course of the EKF (ANN-EKF).

2.1.1 Robot Arm

Robot arms are a serial chain of rigid bodies connected by rotary joints. On basis of a serial chain of six rotary joints $\boldsymbol{\theta}$, as presented in Eq. 1, any robot pose ${}^{R}\boldsymbol{T}_{RF}$ can be approached in the working area of the robot arm. The robot pose ${}^{R}\boldsymbol{T}_{RF}$ consists of position ${}^{R}\boldsymbol{t}_{RF}$ and orientation ${}^{R}\boldsymbol{R}_{RF}$ of the robot flange RF with respect to the robot base frame R. Homogeneous transformations ${}^{R}\boldsymbol{T}_{RF(4\times4)}$ are used for this purpose. For the description of this kinematic robot arm model, we rely on the Denavit-Hartenberg ($\boldsymbol{dh}$) parametrisation (see [29] or [6]). Each transformation requires four parameters: $a_i, \alpha_i, d_i, \theta_i$, whereby only the joint positions $\boldsymbol{\theta}$ vary for each robot pose.

$$\begin{aligned}\begin{bmatrix} {}^{R}\boldsymbol{R}_{RF} & {}^{R}\boldsymbol{t}_{RF} \\ \boldsymbol{0} & 1 \end{bmatrix} &= {}^{R}\boldsymbol{T}_1\,{}^{1}\boldsymbol{T}_2\,{}^{2}\boldsymbol{T}_3\,{}^{3}\boldsymbol{T}_4\,{}^{4}\boldsymbol{T}_5\,{}^{5}\boldsymbol{T}_{RF} \\ &= f(\boldsymbol{a}, \boldsymbol{\alpha}, \boldsymbol{d}, \boldsymbol{\theta})\end{aligned} \tag{1}$$

The quality of the robot pose approached, is the result of the description quality of all influencing variables - from the structure and geometry of the robot arm to the properties of the installed mechanical components. A common categorisation of the error influences is divided into geometric and non-geometric errors. Geometric errors are due to inadequacies of the $\boldsymbol{dh}$ parameters. Non-geometric errors occur during movement and under load. These include the joint compliance, the gear backlash, gear friction, deflection of the arms or the heating of components [30].

2.1.2 ANN

Artificial neural networks are universal and flexible deployable approximating functions. A brief description of how ANNs work is given. For a detailed introduction see [31]. The mathematical notation of a fully connected ANN with one processing hidden layer m is shown in Eq. 2. The function f_n contains K free weights $\boldsymbol{w} = [w_k]$, which must be estimated. Based on the inputs $u_l(t)$ with $l = 1, \ldots, L$ and the initial values of the weights $\boldsymbol{w}_0 = \left[\boldsymbol{w}_{ml,0}; \boldsymbol{w}_{nm,0}\right]$, the output $\hat{v}_n(t)$ with $n = 1, \ldots, N$ is calculated. The activation functions φ are the basis functions of neural networks (see [32]). t is the specific index for the training data sample. The computed output $f_n\left(\boldsymbol{w}_i, \boldsymbol{u}(t)\right)$ is compared to the observed one $v_n(t)$ and the error $e_n(t)$ is back propagated through the network to update the weights $\hat{\boldsymbol{w}}_i$ per iteration i such that the total error ε_i (3) is minimised.

$$\begin{aligned} e_{n,i}(t) &= v_n(t) - \hat{v}_{n,i}(t) = v_n(t) - f_n\left(\boldsymbol{w}_i, \boldsymbol{u}(t)\right) \\ &= v_n(t) - \varphi^{(n)}\left(\sum_m w_{nm,i}\varphi^{(m)}\left(\sum_l w_{ml,i}u_l(t)\right)\right) \end{aligned} \tag{2}$$

$$\varepsilon_i(t) = \frac{1}{2}\sum_n e_{n,i}^2(t) \tag{3}$$

2.1.3 ANN-EKF

The extended Kalman Filter is a linearised recursive data processing algorithm that combines a physical problem description with related observations [33]. The combination of EKF and ANN can be found in [34]. The approach bases on a static system (4). The ANN is considered in the observation (5), which relates the ANN's function $\boldsymbol{h}$ to the observation noise $\boldsymbol{o}(t)$ and the observations $\boldsymbol{y}(t)$. The process noise $\boldsymbol{p}$ and the observation noise $\boldsymbol{o}$ are assumed to be Gaussian with zero mean and the appropriate covariance $\boldsymbol{\Sigma}$. A transition to cofactor matrices $\boldsymbol{Q}$ is fulfilled on basis of the common variance factor of unit weight σ_0^2 ($\boldsymbol{\Sigma} = \sigma_0^2\,\boldsymbol{Q}$).

$$\bar{\boldsymbol{x}}_{i+1} = \boldsymbol{I}\hat{\boldsymbol{x}}_i + \boldsymbol{p}, \quad \boldsymbol{p} \sim \mathcal{N}\left(0, \boldsymbol{\Sigma}_{pp}\right) \tag{4}$$

$$\boldsymbol{y}(t) - \boldsymbol{o}(t) = \boldsymbol{h}\left(\hat{\boldsymbol{x}}_{i+1}, \boldsymbol{u}(t)\right), \quad \boldsymbol{o} \sim \mathcal{N}\left(0, \boldsymbol{\Sigma}_{yy}\right) \tag{5}$$

The ANN expressed in a linear form is: $\boldsymbol{h}\left(\bar{\boldsymbol{x}}_{i+1}, \boldsymbol{u}(t)\right) = \boldsymbol{H}_{i+1}\bar{\boldsymbol{x}}_{i+1}$. The Jacobian matrix $\boldsymbol{H}_{i+1}$ describes the linear relation between the ANN's output and the weights $\boldsymbol{w}$ expressed in the state vector $\boldsymbol{x}$ [27].

Due to the static system, the predicted weights $\bar{\boldsymbol{x}}$ correspond to the preliminary estimated one (4). However, the cofactor matrix of the predicted state $\boldsymbol{Q}_{\bar{x}\bar{x},i+1}$ needs to be computed because of the consideration of the process cofactor matrix $\boldsymbol{Q}_{pp}$ (6). The state estimate is updated on the predicted weights $\bar{\boldsymbol{x}}_{i+1}$ and innovations $\boldsymbol{e}_{i+1}$, weighted by $\boldsymbol{K}_{i+1}$ for each t or batches of t, see Eq. 7. The innovations $\boldsymbol{e}$ (expression in the brackets in Eq. 7) are computed on basis of the non-linear function $\boldsymbol{h}$ of the ANN and corresponds to the error in the ANN estimation (2). The Kalman gain $\boldsymbol{K}_{i+1}$ given in Eq. 8 describes the influence of the observations on the state estimation. If the elements of $\boldsymbol{Q}_{yy}$ are small, i.e. the observations are precise, the Kalman gain $\boldsymbol{K}_{i+1}$ becomes large and consequently the innovation $\boldsymbol{e}$ contributes strongly to the state update. This is controlled by adjusting the variance factor $q_{yy,i}$ on the basis of a compatibility test in which the consistency of the functional and stochastic model is verified (see [27]). The result of the variance propagation is also

a cofactor matrix of the estimated states $\boldsymbol{Q}_{\hat{x}\hat{x},i+1}$ (9) [27].

$$\boldsymbol{Q}_{\bar{x}\bar{x},i+1} = \boldsymbol{I}\,\boldsymbol{Q}_{\hat{x}\hat{x},i}\boldsymbol{I}^T + \boldsymbol{Q}_{pp} \tag{6}$$

$$\hat{\boldsymbol{x}}_{i+1} = \bar{\boldsymbol{x}}_{i+1} + \boldsymbol{K}_{i+1}\Big(\boldsymbol{y}(t) - \boldsymbol{h}\left(\bar{\boldsymbol{x}}_{i+1}, \boldsymbol{u}(t)\right)\Big) \tag{7}$$

$$\boldsymbol{K}_{i+1} = \boldsymbol{Q}_{\bar{x}\bar{x},i+1}\boldsymbol{H}_{i+1}^T \Big(q_{yy,i}\,\tilde{\boldsymbol{Q}}_{yy,i+1} + \boldsymbol{H}_{i+1}\,\boldsymbol{Q}_{\bar{x}\bar{x},i+1}\boldsymbol{H}_{i+1}^T\Big)^{-1} \tag{8}$$

$$\boldsymbol{Q}_{\hat{x}\hat{x},i+1} = \boldsymbol{Q}_{\bar{x}\bar{x},i+1} - \boldsymbol{K}_{i+1}\boldsymbol{H}_{i+1}\,\boldsymbol{Q}_{\bar{x}\bar{x},i+1} \tag{9}$$

2.2 Position Correction Model

The position correction model (PCM) first set up in [27] consists of two components as pictured in Fig. 1: The ANN, which is the core of the PCM, and a preceding transformation (Trafo). It is based on measurements with a laser tracker and a probe, mounted on the robot, which enables measurement in six degrees of freedom. On basis of the robot positions ${}^{R}\boldsymbol{t}_{RF}$ and the laser tracker poses ${}^{LT}\boldsymbol{T}_{P}$, the transformation of the laser tracker with respect to the robot frame ${}^{R}\boldsymbol{T}_{LT}$ as well as the lever arm offset ${}^{P}\boldsymbol{t}_{RF}$ are estimated simultaneously. The transformation model is presented in Eq. 10 and pictured in Fig. 2.

$${}^{R}\boldsymbol{t}_{RF} = {}^{R}\boldsymbol{R}_{LT}\left({}^{LT}\boldsymbol{R}_{P}\,{}^{P}\boldsymbol{t}_{RF} + {}^{LT}\boldsymbol{t}_{P}\right) + {}^{R}\boldsymbol{t}_{LT} \tag{10}$$

Hence, the position corrections ${}^{R}\boldsymbol{\delta t}_{RF}$ can be computed (${}^{R}\boldsymbol{\delta t}_{RF} = {}^{R}\boldsymbol{t}_{RF} - {}^{R}\boldsymbol{t}_{RF,LT}$) as the difference between the robot position ${}^{R}\boldsymbol{t}_{RF}$ and the one derived by the transformed measured robot position ${}^{R}\boldsymbol{t}_{RF,LT}$ according to the right side of Eq. 10. The position correction is the output in the ANN. As a simple ANN model the position corrections ${}^{R}\boldsymbol{\delta t}_{RF}$ are

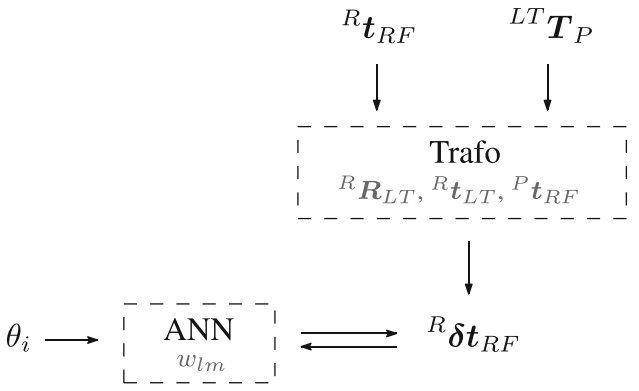

Fig. 1 Position correction model

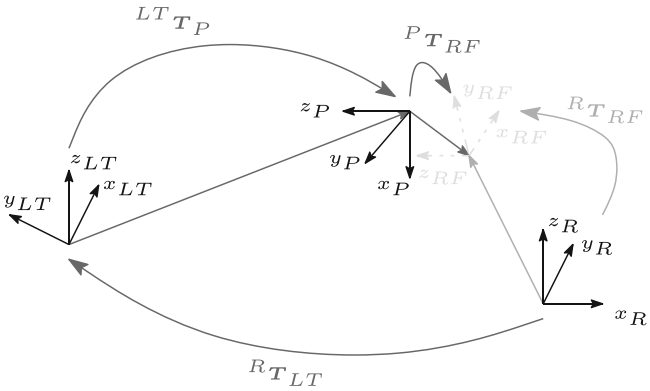

Fig. 2 Relation of robot frame ${}^{R}\boldsymbol{T}_{RF}$ and laser tracker frame ${}^{LT}\boldsymbol{T}_{P}$

determined in dependency of the joints θ_i (see Fig. 1). All causes which lead to a systematic effect due to varying joints are modelled by the parameters of the ANN.

In the first part the simulated data set is discussed. The second part deals with the influence of an insufficient robot model on the estimation results for the transformation and the ANN. Finally, corrective modelling approaches are evaluated.

2.2.1 Data

On basis of simulated data, the effect studies (Sec. 2.2.2, 2.2.3) are performed and the integrated model (Sec. 2.3.2) is validated. The purpose of the simulations requires different data sets. While a good spatial distribution based on randomly chosen poses in the robot working area is important for the effect study, a continuous robot trajectory is required for the validation of the integrated method. Both data sets correspond to a realistic acquisition geometry - line of sights to the laser tracker are taken into account.

For the effect studies in Sections 2.2.2 and 2.2.3, randomised robot arm positions were chosen to achieve a good distribution of robot pose deviations. The randomised robot arm positions used (black vectors) are shown in Fig. 3.

The assessment of the results of the method development in Section 2.3.2 requires a continuous trajectory that also includes non-geometric effects. A trajectory was therefore created in the 'RoboDK' software package and is shown in Fig. 4. It was chosen so that systematic deviations in the geometric or non-geometric model are clearly noticeable. These can occur when the robot arm is in an outstretched and very exposed position. The simulated trajectory of the robot arm is based on the geometric model, which is realised by the $\boldsymbol{dh}$ parameters. The non-geometric effects are simulated by an ANN, trained on real position corrections of the robot arm. The shallow ANN has one hidden layer with 29 hidden nodes. These are tanh activated. The number of hidden nodes were verified in a cross validation and was

limited by Widrow's rule of thumb [32]. The predicted position corrections are presented in Fig. 4 and the color code corresponds to the magnitude of the position corrections 100 times enlarged ($|^R\boldsymbol{\delta t}_{RF}|$). The variation of all simulated position corrections amount to $0.6\,mm$. Considering only the test data, the last approximately 1500 data samples (data sample 5800 to 7300), the position correction varies only about 0.4 mm.

2.2.2 Influence of Model Biases on the PCM

The aim of the PCM is to non-parametrically model the robot arm deviations. The transformation precedes the actual modelling by the ANN. The inputs of the transformation are the robot positions $^R\boldsymbol{t}_{RF}$, which base on the theoretical geometrical robot model and the measured 'true' robot poses $^{LT}\boldsymbol{T}_P$ (see Fig. 1). Consequently, the discrepancy between the theoretical geometric robot arm model and the 'true' robot poses enter into the transformation. The required optimality in the estimation of the transformation and lever arm parameters ($^R\boldsymbol{T}_{LT}$, $^P\boldsymbol{t}_{RF}$) already leads to a modelling/averaging of these discrepancies. In this subsection, the influences of biased $\boldsymbol{dh}$ parameters on the estimation results for the transformation and lever arm parameters as well as the effect on the ANN shall be figured out.

A simulation, biasing each $\boldsymbol{dh}$ parameter separately, serves for the following findings.

Firstly, the influences on the transformation and lever arm parameter shall be evaluated. Therefore, the d_1-parameter is biased for example. In Fig. 3, the robot positions (black vectors) used for this investigation are pictured. The scaled deviations in each robot position show the effect of the bias.

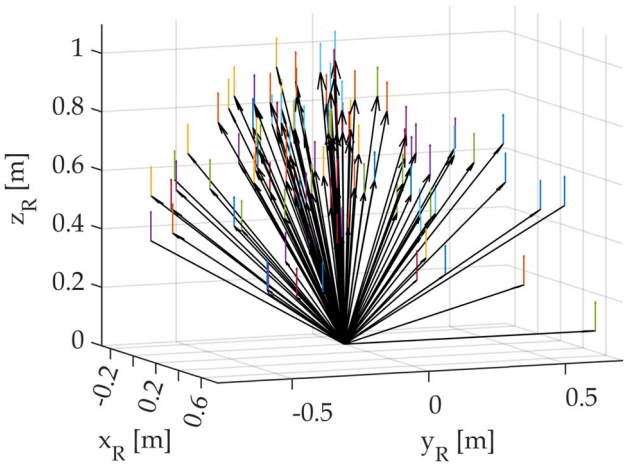

Fig. 3 Robot positions (black vectors) as well as the scaled deviations (coloured small vectors) due to a bias of 0.1 mm for the $\boldsymbol{dh}$ parameter d_1. The measured robot positions refer to the end position of the deviation vectors. Consequently, the estimated transformation parameters are shifted in the z-direction

The measured robot positions refer to the end position of the scaled deviations. Consequently, if the d_1-parameter is not adjusted correctly, the origin of the robot frame will shift upwards when the transformation parameters are calculated based on these 'identical' points (robot positions according to the actual robot model and measured 'nominal' robot positions).

On basis of a Monte-Carlo simulation, each measure is biased by a specified value corresponding to measurement noise or production tolerances one at the time. For metric measures ($\boldsymbol{a}$, $\boldsymbol{d}$) a standard deviation σ_{metr} of 0.1 mm is assumed and the standard deviation of angles σ_{ang} ($\boldsymbol{\alpha}$, $\boldsymbol{\delta\theta}$) amounts to 0.01° respectively 36″.

The mean deviation of the computed transformation and lever arm parameters to the nominal ones is shown in Table 1. Biases in $\boldsymbol{dh}$ parameters at the beginning of the serial chain show more distinct effects on the transformation and lever arm parameters than in the end. The largest mean deviations in $^R\boldsymbol{T}_{LT}$ amounting to 0.5 mm are derived by biases in the following $\boldsymbol{dh}$ parameters: $d\theta_1, d_2, d_3, d_4, d\theta_2, \alpha_1$. The lever arm $^P\boldsymbol{t}_{RF}$ is mainly influenced (approximatley 0.1 mm) by biases in a_6, d_6, a_4. Thus, biased parameters of the robots geometric model are absorbed by the transformation parameters.

Secondly, we want to address the effects of the inadequately modelled robotic arm on the ANN. Therefore, the nominal deviations of the robot arm $^R\boldsymbol{\delta t}_{RF_{nom}}$ are contrasted by the transformed ones $^R\boldsymbol{\delta t}_{RF}$. In Fig. 5, the average deviations for each biased $\boldsymbol{dh}$ parameter ($mean(|^R\boldsymbol{\delta t}_{RF_{nom}}|)$) for all simulated poses (see Fig. 3) are pictured. In contrast to this, the average deviations after the transformations $mean(|^R\boldsymbol{\delta t}_{RF}|)$ are illustrated. We notice, that the bias of these parameters: $d\theta_1, d_1, d\theta_6, d_6, \alpha_6, a_6$ do not cause a deviation after the transformation. Thus, they are absorbed into the transformation and lever arm parameters. Therefore, we treat them as 'absorbed' deviations ($mean(|^R\boldsymbol{\delta t}_{RF}|) = 0$). The listed $\boldsymbol{dh}$ parameters refer to the first or the last joint. The parameters of the first joint interact with the transformation

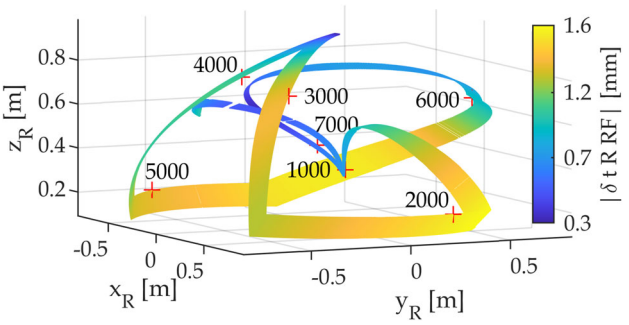

Fig. 4 Simulated robot trajectory inclusive the position corrections predicted by the ANN (100 times enlarged). The marked data samples show the course of the trajectory (from 1000 to 7000)

Table 1 Mean deviations of the estimated transformation and lever arm parameters (${}^{R}\boldsymbol{T}_{LT}, {}^{P}\boldsymbol{t}_{RF}$) due to biases in the kinematic robot parameters ($\boldsymbol{dh}$). Therefore, each parameter is biased by $\sigma_{metr} = 0.1$ mm ($\boldsymbol{a}, \boldsymbol{d}$) or $\sigma_{ang} = 36''$ ($\boldsymbol{\alpha}, \boldsymbol{\delta\theta}$) correspondingly in the Monte Carlo simulation

Par.	${}^{R}\delta\boldsymbol{t}_{LT,x}$	${}^{R}\delta\boldsymbol{t}_{LT,y}$	${}^{R}\delta\boldsymbol{t}_{LT,z}$	${}^{R}\delta\boldsymbol{R}_{LT,x}$	${}^{R}\delta\boldsymbol{R}_{LT,y}$	${}^{R}\delta\boldsymbol{R}_{LT,z}$	${}^{P}\delta\boldsymbol{t}_{RF,x}$	${}^{P}\delta\boldsymbol{t}_{RF,y}$	${}^{P}\delta\boldsymbol{t}_{RF,z}$
a_1	$0.1mm$	$0.1mm$	$0.1mm$	$4''$	$3''$	$10''$	$0mm$	$0mm$	$0mm$
a_2	$0mm$	$0mm$	$0.1mm$	$3''$	$2''$	$1''$	$0mm$	$0mm$	$0mm$
a_3	$0.1mm$	$0.1mm$	$0.1mm$	$5''$	$4''$	$7''$	$0mm$	$0mm$	$0mm$
a_4	$0.1mm$	$0.1mm$	$0mm$	$2''$	$3''$	$10''$	$0mm$	$0mm$	$0.1mm$
a_5	$0.1mm$	$0.2mm$	$0mm$	$7''$	$4''$	$12''$	$0mm$	$0mm$	$0mm$
a_6	$0mm$	$0mm$	$0mm$	$0''$	$0''$	$0''$	$0.1mm$	$0mm$	$0mm$
d_1	$0mm$	$0mm$	$0.1mm$	$0''$	$0''$	$0''$	$0mm$	$0mm$	$0mm$
d_2	$0.3mm$	$0.4mm$	$0.0mm$	$3''$	$3''$	$33''$	$0mm$	$0mm$	$0mm$
d_3	$0.3mm$	$0.4mm$	$0mm$	$3''$	$3''$	$33''$	$0mm$	$0mm$	$0mm$
d_4	$0.3mm$	$0.4mm$	$0mm$	$3''$	$3''$	$33''$	$0mm$	$0mm$	$0mm$
d_5	$0mm$	$0mm$	$0.2mm$	$10''$	$2''$	$2''$	$0mm$	$0mm$	$0mm$
d_6	$0mm$	$0mm$	$0mm$	$0''$	$0''$	$0''$	$0mm$	$0mm$	$0.1mm$
α_1	$0.2mm$	$0.3mm$	$0.1mm$	$6''$	$1''$	$23''$	$0mm$	$0mm$	$0mm$
α_2	$0.1mm$	$0.2mm$	$0.1mm$	$1''$	$6''$	$13''$	$0mm$	$0mm$	$0mm$
α_3	$0mm$	$0mm$	$0.1mm$	$2''$	$6''$	$2''$	$0mm$	$0mm$	$0mm$
α_4	$0mm$	$0.1mm$	$0mm$	$1''$	$1''$	$5''$	$0mm$	$0mm$	$0mm$
α_5	$0mm$	$0mm$	$0mm$	$1''$	$0''$	$0''$	$0mm$	$0mm$	$0mm$
α_6	$0mm$	$0mm$	$0mm$	$0''$	$0''$	$0''$	$0mm$	$0mm$	$0mm$
$\delta\theta_1$	$0.3mm$	$0.5mm$	$0mm$	$0''$	$0''$	$36''$	$0mm$	$0mm$	$0mm$
$\delta\theta_2$	$0.1mm$	$0.1mm$	$0.4mm$	$10''$	$25''$	$8''$	$0mm$	$0mm$	$0mm$
$\delta\theta_3$	$0mm$	$0mm$	$0.3mm$	$5''$	$13''$	$3''$	$0mm$	$0mm$	$0mm$
$\delta\theta_4$	$0mm$	$0mm$	$0mm$	$1''$	$0''$	$2''$	$0mm$	$0mm$	$0mm$
$\delta\theta_5$	$0mm$	$0mm$	$0mm$	$1''$	$1''$	$2''$	$0mm$	$0mm$	$0mm$
$\delta\theta_6$	$0mm$	$0mm$	$0mm$	$0''$	$0''$	$0''$	$0mm$	$0mm$	$0mm$
all	$0.6mm$	$0.9mm$	$0.5mm$	$0''$	$0''$	$0''$	$0.1mm$	$0mm$	$0.1mm$

parameters ${}^{R}\boldsymbol{R}_{LT,z}$ and ${}^{R}\boldsymbol{t}_{LT,z}$. The parameters of the last joint act similar to the lever arm ${}^{P}\boldsymbol{t}_{RF}$.

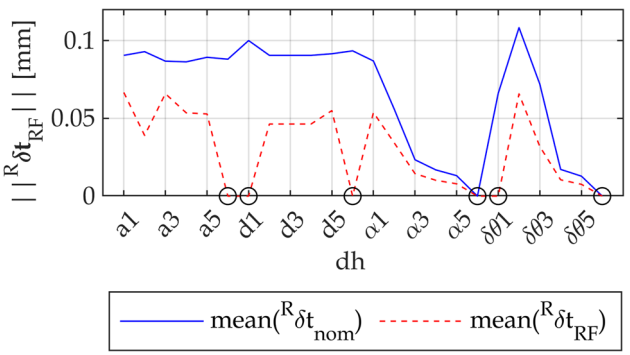

Fig. 5 'Absorbed' deviations of the kinematic robot parameter by the transformation ($mean(|{}^{R}\boldsymbol{\delta t}_{RF}|) = 0$; black circles) and 'remaining' deviations to be modelled by the ANN ($mean(|{}^{R}\boldsymbol{\delta t}_{RF}|) \neq 0$)

In contrast, the transformed deviations of the 'remaining' parameters ($mean(|{}^{R}\boldsymbol{\delta t}_{RF}|) \neq 0$) amount to approximately 60% of the nominal deviations. Consequently, in average approximately 40% of the robot position deviations are absorbed by the transformation. While the nominal position deviation $|{}^{R}\boldsymbol{\delta t}_{RF\,nom}|$ for parameter a_1 is about 0.09 mm, the transformed one $|{}^{R}\boldsymbol{\delta t}_{RF}|$ results in 0.065 mm according Fig. 5.

The aim of the PCM is to improve the system robot arm. As we have shown so far, some of the position corrections are completely absorbed or mitigated due to the preceding transformation. The 'lost' resp. 'absorbed' parameters can only be evaluated separately by special measurement routines and not in a joint evaluation with the transformation and the lever arm. The focus of the following investigations is to keep the complete 'remaining' parameters: a_1-a_5, d_2-d_5, α_1-α_5, $\delta\theta_2$-$\delta\theta_5$.

2.2.3 Reducing Model Biases

A suggestion to obtain less biased transformation and lever arm parameters is to estimate the transformation and lever arm parameters in the course of a kinematic robot arm calibration, as done in literature ([10, 15, 25]).

The corresponding model is presented in Eq. 11. In addition to the robot parameters ($\boldsymbol{dh}$), the transformation between the robot base frame and the laser tracker ${}^{LT}\boldsymbol{T}_R$ and the translation between the probe and the robot flange ${}^{RF}\boldsymbol{t}_P$ (lever arm) must be determined.

$$\begin{bmatrix} {}^{LT}\boldsymbol{t}_P \\ 1 \end{bmatrix} = {}^{LT}\boldsymbol{T}_R \cdot f(\boldsymbol{a}, \boldsymbol{\alpha}, \boldsymbol{d}, \boldsymbol{\theta} + \boldsymbol{\delta\theta}) \cdot \begin{bmatrix} {}^{RF}\boldsymbol{t}_P \\ 1 \end{bmatrix} \tag{11}$$

Due to a similar impact of some parameters linear dependencies appear. These exist here for the following parameter groups: $\{\delta\theta_1, {}^{LT}\boldsymbol{r}_{R,z}\}$, $\{d_1, {}^{LT}\boldsymbol{t}_{R,z}\}$ $\{d_2, d_3, d_4\}$, $\{a_6, {}^{RF}\boldsymbol{t}_{P,x}\}$, $\{d_6, {}^{RF}\boldsymbol{t}_{P,z}\}$ and $\{\alpha_6, \delta\theta_6, {}^{RF}\boldsymbol{t}_{P,y}\}$ (see [35]). The linear dependencies corresponding to the transformation parameters ${}^{LT}\boldsymbol{T}_R$ originate due to a vertical alignment of the laser tracker z-axis and the robot arm z-axis.

It can be noticed that the 'absorbed' $\boldsymbol{dh}$ parameters identified in Section 2.2.2 correspond to the linear dependent ones in the kinematic robot arm calibration. Consequently, the linear dependencies in the kinematic calibration confirm the results of how biases in $\boldsymbol{dh}$ parameters affect the estimation of transformation and lever arm.

As the focus lies on the estimation of the transformation and the lever arm, we select out of the parameter groups ${}^{LT}\boldsymbol{r}_{R,z}, {}^{LT}\boldsymbol{t}_{R,z}, {}^{RF}\boldsymbol{t}_{P,x}, {}^{RF}\boldsymbol{t}_{P,z}, {}^{RF}\boldsymbol{t}_{P,y}$ to be estimated. In contrast to the kinematic calibration, where the $\boldsymbol{dh}$ parameter are of interest, here the focus is set on the transformation and the lever arm components. Therefore, the following $\boldsymbol{dh}$ parameters will be set constant: $d_1, d_3, d_4, d_6, \delta\theta_1, \delta\theta_6, \alpha_6, a_6$, instead of the appropriate transformation parameters. A bias of their true values to the model shifts in the appropriate transformation and lever arm parameter.

On the basis of the findings in Section 2.2.2, three types of simulations in the kinematic calibration model are established - either only the 'remaining' parameters, only the 'absorbed' ones or 'all' parameters are biased together. Therefore, the metric measures are biased by $\sigma_{metr} = 0.1$ mm and the angles by $\sigma_{ang} = 0.01°$, similar to the Monte Carlo simulations of Section 2.2.2. Again, the mean deviations of the transformation and lever arm parameters after the kinematic calibration are analysed. The results of the kinematic calibration model by biasing all parameters of a group are presented in Table 2. First, only the 'remaining' parameters (a_1-a_5, d_2-d_5, α_1-α_5, $\delta\theta_2$-$\delta\theta_5$) are biased. No deviations in the transformation and lever arm parameter occur - the correct parameter can be figured out by the kinematic calibration. In a next step, only the 'absorbed' parameters ($d\theta_1, d_1, d\theta_6, d_6, \alpha_6, a_6$) are biased. This creates mean deviations in the following components: ${}^{R}\delta\boldsymbol{t}_{LT,z}$, ${}^{P}\delta\boldsymbol{t}_{RF,x}$ and ${}^{P}\delta\boldsymbol{t}_{RF,z}$. The 'absorbed' $\boldsymbol{dh}$ parameters correspond to the linear dependent ones in the kinematic calibration and have been set constant. Consequently, biases in these parameters enter in the transformation and lever arm parameters. If 'all' parameters are biased, the same mean deviations are reached as in the 'absorbed' case. The main deviations influence the z-translation ${}^{R}\delta\boldsymbol{t}_{LT,z}$ as well as the lever arm x- and z-component ${}^{P}\delta\boldsymbol{t}_{RF,x}$, ${}^{P}\delta\boldsymbol{t}_{RF,z}$. The estimated parameters are larger than the simulated ones due to an enlargement of the aforementioned parameters.

Comparing the result of biasing 'all' $\boldsymbol{dh}$ parameters in the kinematic calibration (Table 2) to the result of biasing 'all' $\boldsymbol{dh}$ parameters in the PCM model (Table 1) shows less deviations in the transformation and lever arm parameters. Thus, less biased transformation and lever arm parameters are obtained by the kinematic calibration approach.

Therefore, a kinematic calibration is performed first, from which the transformation and lever arm parameters are used to calculate the deltas for the non-parametric estimation in the ANN (see Fig. 6 our so called 'kinCalib+' approach). This approach is a common method that has been used repeatedly in literature ([10, 15, 24] and [25]). The idea is to perform geometric modelling and apply non-parametric methods to estimate the remaining deviations.

However, the results of our kinematic calibration of a collaborative robot arm showed shortcomings. The goodness-of-fit test according to [36] could not be passed due to a

Table 2 Mean deviations in the transformation and lever arm parameters (${}^{R}\boldsymbol{T}_{LT}, {}^{P}\boldsymbol{t}_{RF}$) due to biases in the kinematic robot parameters ($\boldsymbol{dh}$). In contrast to Table 1, the kinematic calibration model (Eq. 11) is applied in the Monte Carlo simulation. Consequently, the deviations caused by a biased $\boldsymbol{dh}$ parameter enter in the appropriate parameter except the absorbing ones (compare to Section 2.2.2). The table shows three variants of biased parameters: the 'remaining', the 'absorbed' or 'all' parameters. The estimated parameters are larger than the simulated ones

Par.	${}^{R}\delta\boldsymbol{t}_{LT,x}$	${}^{R}\delta\boldsymbol{t}_{LT,y}$	${}^{R}\delta\boldsymbol{t}_{LT,z}$	${}^{R}\delta\boldsymbol{R}_{LT,x}$	${}^{R}\delta\boldsymbol{R}_{LT,y}$	${}^{R}\delta\boldsymbol{R}_{LT,z}$	${}^{P}\delta\boldsymbol{t}_{RF,x}$	${}^{P}\delta\boldsymbol{t}_{RF,y}$	${}^{P}\delta\boldsymbol{t}_{RF,z}$
remaining	$0mm$	$0mm$	$0mm$	$0''$	$0''$	$0''$	$0mm$	$0mm$	$0mm$
absorbed	$0.3mm$	$0.4mm$	$0.1mm$	$0''$	$0''$	$0''$	$0mm$	$0mm$	$0mm$
all	$0.3mm$	$0.5mm$	$0.1mm$	$0''$	$0''$	$0''$	$0mm$	$0mm$	$0mm$

greatly increased test measure by an order of magnitude of 10^3 [35]. The reason for this can be found in an inadequate functional model. Due to a good knowledge of the quality of the laser tracker measurements and outlier detection, an inadequate stochastic model of the observations and outliers can be excluded as causes. Consequently, the non-geometrical effects need to be considered jointly with the geometrical ones. It prompts us to go one step further than the 'kinCalb+' model ([10, 15, 24] and [25]) and to develop the simultaneous estimation of the kinematic model parameters and the ANN ('Integrated' model in Fig. 6).

Aim of the simultaneous estimation of geometrical and non-geometrical model parameters for a robot arm is to reduce the residuals and to pass the goodness-of-fit test for the selected robot arm model. Thereby, a realistic modelling of the robot arm is achieved - systematic effects are assigned according to their origin or mode of action. The integration of the geometric and non-geometric methods is introduced in the next section.

2.3 Integration Kinematic Model in ANN-EKF

In general, the KF approach combines a dynamic system description with measurements. So far, we have only used the KF as an optimisation method for ANN estimation. The idea to integrate system knowledge i.e. the robot geometric description in the system description lends itself. Thereby, the non-parametric ANN world and the parametric KF world are combined towards a hybrid modelling approach.

In Section 2.3.1 the basic concepts for integrating the geometric and non-geometric part are discussed, before the integrated model is presented in Section 2.3.2.

2.3.1 Basic Concepts of the Integration

The main problem of the PCM is the sequential procedure - systematic effects of the robot arm are already masked by the preceding transformation (see Section 2.2.2). Thus, the basic idea is to facilitate the estimation of all parameters at once by the integration of parametric and non-parametric system description in the framework of KF. The EKF enables an additional estimation of a priori poorly known parameters of the functional or of the stochastical model in course of an adaptive filtering. For a future adaptive estimation it is important that the parameters are considered already in the appropriate way. According to that, the robot model parameter $\boldsymbol{dh}$, the transformation and lever arm parameters ${}^{R}\boldsymbol{T}_{LT}$, ${}^{RF}\boldsymbol{t}_{P}$ need to be included in the system description of the filter.

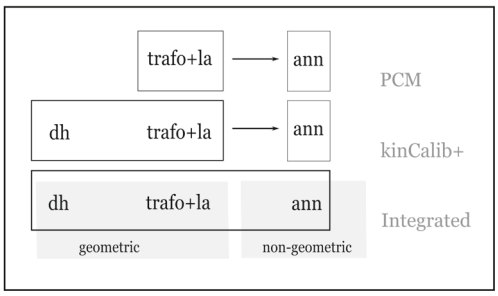

Fig. 6 Extensions of the position correction model (PCM)

Another basic concept results from the static measurements, which were retained to be consistent with preliminary work [27]. Consequently, the kinematic system description was adapted to the static measurements. In the standard case of Kalman filter theory, the states model the actual dynamics of a system, while the control variables model additional deterministic effects. Considering this, the state $\boldsymbol{x}$ consists of the robot position expressed as the position of the probe in the laser tracker system ${}^{LT}\boldsymbol{t}_{P}$ and the ANN parameters $\boldsymbol{w}$. The prediction from the actual state ${}^{LT}\boldsymbol{t}_{P,i}$ to the next state ${}^{LT}\boldsymbol{t}_{P,i+1}$ is enabled by the present joints $\boldsymbol{\theta}_i$ and the subsequent joints $\boldsymbol{\theta}_{i+1}$, contained in the control variable $\boldsymbol{u}$.

The formulation of the ANN in the filter approach forms the third basic concept. The ANN is kept in the observation (5), so the parameters $\boldsymbol{w}_i$ are determined according to the deviation between measurement and estimated ANN output. This adaptation is reached by the update rule of the Kalman filter (7), if the ANN parameters $\boldsymbol{w}_i$ are treated as static states (4).

The observation refers to the superposition of the geometric and non-geometric part (12). The geometric part is parameterised in the system description. The non-geometric part realised by the ANN must take into account all systematic (non-geometric) effects that cannot be explained by the kinematic robot model.

$$\boldsymbol{obs} = \boldsymbol{geom} + \boldsymbol{non\text{-}geom} \tag{12}$$

Thereby, the observation equation combines the parametric KF world and the non-parametric ANN world.

Due to the geometric problem description only additive white Gaussian noise is assumed in the following. Considering these concepts, leads to the formulation of the model in the following subsection.

2.3.2 Integrated Model

As stated in the second basic concept, we need a relative description of the robot arm in order to predict from one robot position i to the subsequent one $i+1$. Eq. 13 presents a relative formulation on basis of homogeneous transformation matrices. According to the second basic concept, the relative

robot description is expressed as a motion of the probe in the LT frame ${}^{LT}\boldsymbol{t}_P$. Hence, the robot model parameter $\boldsymbol{dh}$ as well as the transformation parameters ${}^{LT}\boldsymbol{T}_R$ and lever arm components ${}^{RF}\boldsymbol{T}_P$ are present in the system description, which should enable a future adaptive estimation. However, due to the relative formulation, the transformation of the robot arm into the laser tracker system ${}^{LT}\boldsymbol{T}_R$ cancels out, what contradicts the second basic concept. We will leave it at that for the time being. In the course of future adaptive estimation, the transformation by back-substitution is to find its way back into the system description.

One assumed simplification is that ${}^{RF}\boldsymbol{R}_P = \boldsymbol{I}$, which is the result of the specially designed probe mounting. Future work shall consider the full populated ${}^{RF}\boldsymbol{R}_P$ matrix in the system description.

Further, only the position resp. translational information of the robot is used instead of the complete pose in the filter description, at the moment. Out of ${}^{P,i}\boldsymbol{\Delta T}_{P,i+1}$ in Eq. 13 only the translational part is taken into account and it results in Eq. 14. Thus, the robot position deviation is a function of the $\boldsymbol{dh}$ parameter at time i and time $i+1$ and the lever arm ${}^{RF}\boldsymbol{t}_P$.

$$\begin{aligned} {}^{P,i}\boldsymbol{\Delta T}_{P,i+1} &= {}^{LT}\boldsymbol{T}_{P,i}{}^{-1}\,{}^{LT}\boldsymbol{T}_{P,i+1} \\ &= \left({}^{LT}\boldsymbol{T}_R\,{}^{R}\boldsymbol{T}_{RF,i}\,{}^{RF}\boldsymbol{T}_P\right)^{-1} \\ &\quad \left({}^{LT}\boldsymbol{T}_R\,{}^{R}\boldsymbol{T}_{RF,i+1}\,{}^{RF}\boldsymbol{T}_P\right) \end{aligned} \tag{13}$$

$$\begin{aligned} {}^{P,i}\boldsymbol{\Delta t}_{P,i+1} &= {}^{R}\boldsymbol{R}_{RF,i}{}^{T}\left({}^{R}\boldsymbol{t}_{RF,i+1} - {}^{R}\boldsymbol{t}_{RF,i}\right) \\ &\quad - {}^{RF}\boldsymbol{t}_P + {}^{R}\boldsymbol{R}_{RF,i}{}^{T}\,{}^{R}\boldsymbol{R}_{RF,i+1}\,{}^{RF}\boldsymbol{t}_P \\ &= \boldsymbol{f}_{\Delta t}(\boldsymbol{\theta}_i, \boldsymbol{\theta}_{i+1}, \boldsymbol{a}, \boldsymbol{d}, \boldsymbol{\alpha}, {}^{RF}\boldsymbol{t}_P) \end{aligned} \tag{14}$$

Figure 7 illustrates the relative robot description as formulated in Eq. 14. The relative robot position seen from the measuring system ${}^{P,i}\boldsymbol{\Delta t}_{P,i+1}$ consists of three parts: First, the difference vector ${}^{RF,i}\boldsymbol{\Delta t}_{RF,i+1} = ({}^{R}\boldsymbol{t}_{RF,i+1} - {}^{R}\boldsymbol{t}_{RF,i})$ in regard to the robot frame at time i; second, the leverarm ${}^{RF}\boldsymbol{t}_P$ to transform into the probe system and third, due to the change in robot arm orientation, the component of the rotated leverarm needs to be considered.

Appending the relative robot arm position (14) to the initial robot pose ${}^{LT}\boldsymbol{T}_{P,i}$ enables a prediction of the subsequent robot arm position as presented in Eq. 15. It includes the noise of the estimated state $\boldsymbol{p}_{{}^{LT}\boldsymbol{t}_P}$. Temporally variable quantities in this equation are the joints $\boldsymbol{\theta}_i, \boldsymbol{\theta}_{i+1}$, summarised in the control variable $\boldsymbol{u}$, and the preceding robot pose ${}^{LT}\boldsymbol{T}_{P,i}$, whereby only the position is estimated as a state $\boldsymbol{x}$ and the rotational part ${}^{LT}\boldsymbol{R}_{P,i}$ is treated as a deterministic measure for the time being.

$$\begin{aligned} {}^{LT}\bar{\boldsymbol{t}}_{P,i+1} &= {}^{LT}\boldsymbol{R}_{P,i} \cdot {}^{P,i}\boldsymbol{\Delta t}_{P,i+1} + {}^{LT}\boldsymbol{t}_{P,i} + \boldsymbol{p}_{{}^{LT}\boldsymbol{t}_P} \\ &= \boldsymbol{f}_t({}^{LT}\hat{\boldsymbol{t}}_{P,i}, \boldsymbol{\theta}_i, \boldsymbol{\theta}_{i+1}) + \boldsymbol{p}_{{}^{LT}\boldsymbol{t}_P} \end{aligned} \tag{15}$$

The linearised EKF system (16) consists of the functional $\boldsymbol{f}_t(\hat{\boldsymbol{x}}_i, \boldsymbol{u}_i)$, evaluated at the location of the state estimate $\hat{\boldsymbol{x}}_i$ and on the nominal control $\boldsymbol{u}_i = [\boldsymbol{\theta}_i]$, as well as of the relative robot pose, considered in the control matrix $\boldsymbol{B}$. The linearised model is used for the propagation of the stochastic model. The state prediction is accomplished by the nonlinear model (15).

$$\bar{\boldsymbol{x}}_{i+1} = \underbrace{\boldsymbol{f}_t\left(\hat{\boldsymbol{x}}_i, \boldsymbol{u}_i\right)}_{{}^{LT}\hat{\boldsymbol{t}}_{P,i}} + \underbrace{\frac{\partial \boldsymbol{f}}{\partial \boldsymbol{\theta}_{i+1}}\Big|_{\theta_i} \cdot (\boldsymbol{\theta}_{i+1} - \boldsymbol{\theta}_i)}_{\boldsymbol{B}_i \cdot \boldsymbol{\Delta u}_i} + \boldsymbol{p}_{{}^{LT}\boldsymbol{t}_P} \tag{16}$$

The third basic concept indicates to treat the ANN parameters $\boldsymbol{w}_i$ as states in a static system. Thereby, the adaptation of the ANN parameters is accomplished in dependence of the deviation between the measurements and the ANN outputs. Equation 17 shows the static system including the ANN parameter noise $\boldsymbol{p}_w$.

$$\bar{\boldsymbol{w}}_{i+1} = \boldsymbol{f}_w(\hat{\boldsymbol{x}}_i) + \boldsymbol{p}_w = \hat{\boldsymbol{w}}_i + \boldsymbol{p}_w \tag{17}$$

The complete linearised system is presented in Eq. 18. It includes the linear prediction of the ANN parameters (17) and the robot arm position (16). However, the filter predicts on basis of the non-linear function (15). The partial derivatives

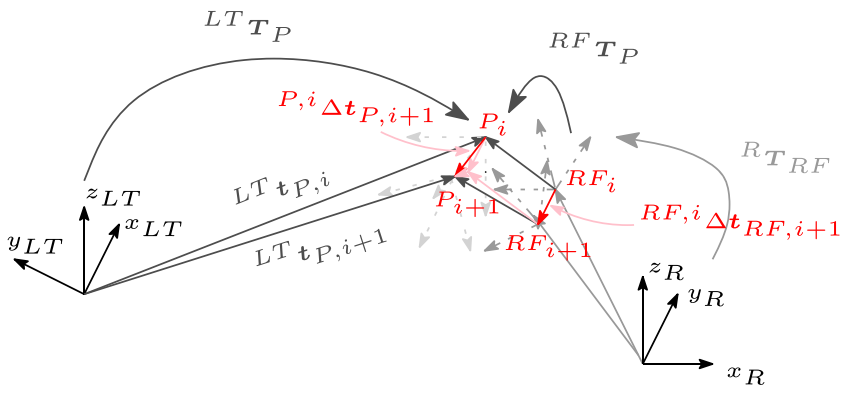

Fig. 7 Scretch of the relative robot model (in red color). The relative robot position in the robot flange frame at time i is denoted by ${}^{RF,i}\boldsymbol{\Delta t}_{RF,i+1}$ and the corresponding relative robot position as seen from the measuring system is denoted by ${}^{P,i}\boldsymbol{\Delta t}_{P,i+1}$

are necessary for the stochastic propagation, as applied in Eq. 19.

$$\bar{\boldsymbol{x}}_{i+1} = \boldsymbol{f}\left(\hat{\boldsymbol{x}}_i, \boldsymbol{u}_i\right) + \boldsymbol{B}_i \cdot \boldsymbol{\Delta u}_i + \boldsymbol{p} \tag{18}$$

$$\underset{(n+3)\times 1}{\begin{bmatrix} \bar{\boldsymbol{w}}_{i+1} \\ {}^{LT}\bar{\boldsymbol{t}}_{P,i+1} \end{bmatrix}} = \underset{(n+3)\times 1}{\begin{bmatrix} \boldsymbol{f}_w\left(\hat{\boldsymbol{x}}_i\right) \\ \boldsymbol{f}_t\left(\hat{\boldsymbol{x}}_i, \boldsymbol{u}_i\right) \end{bmatrix}} + \underset{(n+3)\times 12}{\begin{bmatrix} \boldsymbol{0}_{n\times 6} & \boldsymbol{0}_{n\times 6} \\ \frac{\partial \boldsymbol{f}_t}{\partial \boldsymbol{\theta}_i} & \frac{\partial \boldsymbol{f}_t}{\partial \boldsymbol{\theta}_{i+1}} \end{bmatrix}} \cdot \underset{12\times 1}{\begin{bmatrix} \boldsymbol{0}_{6\times 1} \\ \boldsymbol{\Delta\theta}_{i,i+1} \end{bmatrix}} + \begin{bmatrix} \boldsymbol{p}_w \\ \boldsymbol{p}_{{}^{LT}t_P} \end{bmatrix}$$

$$\boldsymbol{Q}_{\bar{x}\bar{x},i+1} = \boldsymbol{I}\,\boldsymbol{Q}_{\hat{x}\hat{x},i}\boldsymbol{I}^T + \boldsymbol{B}\,\boldsymbol{Q}_{uu}\boldsymbol{B}^T + \boldsymbol{Q}_{pp} \tag{19}$$

The ANN is part of the observation (20). It models the robot position deviations ${}^{R}\boldsymbol{\delta t}_{RF}$ in dependence of its joints $\boldsymbol{\theta}$: ${}^{R}\boldsymbol{\delta t}_{RF,i+1} = \boldsymbol{g}\left(\boldsymbol{\theta}_{i+1}, \bar{\boldsymbol{w}}_{i+1}\right)$.

The rotated ANN describes the non-geometrical part (non-geom) of the robot arm and in prediction mode we call it a 'position correction'. The geometric modelling (geom) originates out of the system description. Both parts add up to the observation: $\boldsymbol{y} = {}^{LT}\boldsymbol{t}_{P,i+1,Obs}$, which embodies the actual value except the observation noise $\boldsymbol{o}_{{}^{LT}t_P}$.

$$\begin{aligned} \boldsymbol{y}_{i+1} &= \boldsymbol{h}(\hat{\boldsymbol{x}}_{i+1}, \boldsymbol{\theta}_{i+1}, {}^{LT}\boldsymbol{R}_R) \\ &= \underbrace{{}^{LT}\hat{\boldsymbol{t}}_{P,i+1}}_{geom} + \underbrace{{}^{LT}\boldsymbol{R}_R \cdot {}^{R}\boldsymbol{\delta t}_{RF,i+1}}_{non\text{-}geom} + \boldsymbol{o}_{{}^{LT}t_P} \end{aligned} \tag{20}$$

The non-linear observation function $\boldsymbol{h}$ is used in the update equation of the Kalman filter (7). However, for the Kalman gain computation (8) and the computation of the updated cofactor matrix of the state (9) the partial derivatives are needed. Equation 21 presents the generic partial derivative of the observation function $\boldsymbol{h}$.

$$\boldsymbol{H} = \frac{\partial \boldsymbol{h}}{\partial \boldsymbol{x}}\Big|_{\bar{\boldsymbol{x}}_{i+1}} \tag{21}$$

The model established hereby is the starting point for the simultaneous estimation of all parameters, which is only achieved by extending the system model with the corresponding parameters in the course of adaptive filtering, which will be part of future work. Here, however, we concentrate on checking the functioning of the model.

3 Results

The focus of this section is on proving the functionality and evaluating the performance of the proposed algorithm. The scenarios used to test the method are shown in Fig. 8. The first scenario describes the ideal case with nominal parameters and only considers the measurement noise. In the second scenario, the functionality of the ANN is proven by some initial

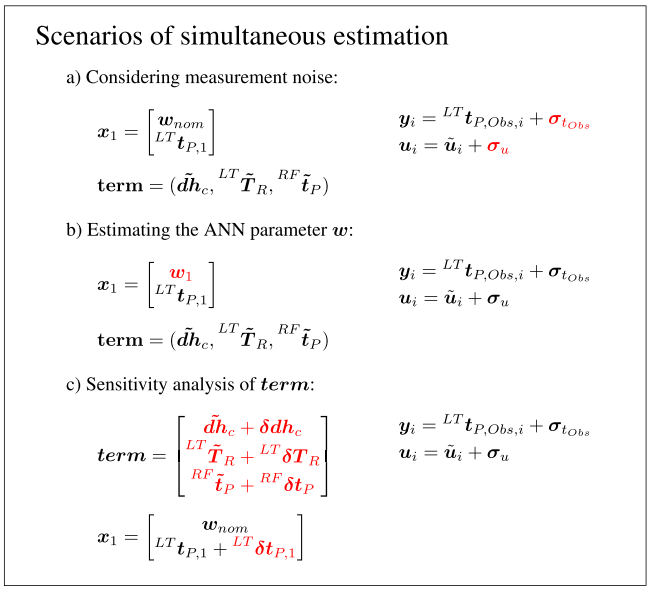

Fig. 8 Scenarios of simultaneous estimation. The variables that are varied or adapted in the course of a scenario are shown in red. (left column: initial state values; right column: observations inclusive noise)

ANN parameters that differ from the nominal ones. Thirdly, a preliminary stage of adaptive estimation is attempted. A sensitivity analysis is performed to check whether the transformation or robot parameter are estimable or observable.

3.1 Considering Measurement Noise

This first scenario describes the ideal case of the proposed model and serves as a proof for the functionality of the algorithm. Therefore, transformation ${}^{LT}\boldsymbol{T}_R$ and lever arm parameters ${}^{RF}\boldsymbol{t}_P$ and constant robot arm parameters like $\boldsymbol{a}, \boldsymbol{d}, \boldsymbol{\alpha}$ are set to their nominal values $({}^{LT}\tilde{\boldsymbol{T}}_R, {}^{RF}\tilde{\boldsymbol{t}}_P, \tilde{\boldsymbol{dh}}_c)$. Measurements like the robot joint positions $\boldsymbol{\theta}_i$ and laser tracker positions ${}^{LT}\boldsymbol{t}_{P,i}$ include noise on a realistic level of robot arms presented in Table 3. The precision of the joints σ_u leads to an average position deviation of 1.5×10^{-5} m. Moreover, the initial guess for the ANN parameters $\boldsymbol{w}_1$ are the ANN parameters of the ANN that simulates the non-geometric component $\boldsymbol{w}_{nom}$ (Section 2.2.1). The model structure was also inherited from this original ANN.

Initialising a Monte Carlo simulation and averaging the 10-fold drawing from the normal distribution with the standard deviation $\boldsymbol{\sigma}_u$ and $\boldsymbol{\sigma}_{tObs}$ leads to the mean deviations presented in Fig. 9. The results are discussed on basis of the components of the integrated model: the geometric part (G), the non-geometric part (NG) and the combination of both (All). The geometric part corresponds to the predicted state, the non-geometric part results out of the ANN and the sum of both components is combined in 'All'. For better interpretability of the results, deviations to their nominal values

are considered. The deviations of the non-geometric part is nearly zero, due to the usage of the nominal ANN parameters. The mean of the geometric (devG) and of the combined part (devAll) is also close to zero, however, the standard deviation of the joints is mainly reflected in the variation of these two components. Due to the optimal description of the ANN, the geometric component mainly influences the filtering process and determines the combined position. The root mean squared error (RMSE) of the combined position (All) corresponds nearly to the level of the assumed standard deviations according to Table 3. The smaller variation of the predicted positions of the test data compared to the trained positions is noticeable, which is caused by the respective position correction (see Fig. 4) and the quality of the estimation of the geometric part. The deviations of the robot arm trajectory (devG, devAll) are in the magnitude of the simulated robot arm position precision. Thus, no systematics are recognisable on this database.

3.2 Estimating ANN Parameters

Till now only nominal ANN parameters $\boldsymbol{w}_{nom}$ have been used. These are the ANN parameters of the simulated non-geometric component (Sec. 2.2.1). It is questionable, if the ANN is estimable on basis of random initialised ANN parameters.

Two important screws enabling the estimation of the ANN parameters are: the stochastic model of the various filter components and an additional ANN iteration. A first test on adapting the stochastic model of the ANN parameter shows that larger initial standard deviations of the ANN parameters $\boldsymbol{\sigma}_w$ lead to changes in the ANN parameters. However, these changes are much too small in magnitude. It seems to need more processing steps in order to model the simulated non-geometric components of the robot arm.

The ANN estimation usually requires many iterations until an adaptation to the observed output is possible. Especially if the initial guess is far away from the target solution, it is particularly important to iterate. Consequently, an additional iteration of the ANN takes into account the adaptive behaviour of ML methods in the state estimation. The implementation of an additional iteration of the ANN demands a redraft or extension of the Kalman filter, which is presented in Fig. 10. The lower part shows the implementation of the integrated approach, whereby the ANN is included in the observation equation $\boldsymbol{h}$. The area in the dashed rectangle extends the integrated approach by the additional iteration of the ANN. This additional iteration process is accomplished after each 500 update steps/data samples up to the end of the training samples N_{tr}. The ANN parameters $\boldsymbol{w}_{i+1}$ are trained on the position corrections ${}^{R}\boldsymbol{\delta t}_{RF,i+1}$ on basis of the inputs $\boldsymbol{\theta}_{i+1}$. Therefore, the position corrections need to be derived (22).

$$
\begin{aligned}
{}^{R}\boldsymbol{\delta t}_{RF,i+1} &= {}^{LT}\boldsymbol{R}_{R}{}^{T} \cdot \left(\boldsymbol{y}_{i+1} - {}^{LT}\bar{\boldsymbol{t}}_{P,i+1}\right) \\
&= \boldsymbol{g}(\boldsymbol{\theta}_{i+1}, \bar{\boldsymbol{w}}_{i+1})
\end{aligned}
\tag{22}
$$

It corresponds to the reformulated observation (20) under ${}^{RF}\boldsymbol{R}_{P} = \boldsymbol{I}$. The resulting ANN parameters $\bar{\boldsymbol{w}}_{i+1,iter}$ are fed back to the integrated approach as a new prediction of the ANN parameter $\bar{\boldsymbol{w}}_{i+1}$. The updating of the ANN is accomplished by Levenberg-Marquardt (LM). Due to the industrial application a stochastic learning procedure is preferable to batch learning [37]. The available data samples in each additional ANN computation step i are shuffled. The quit criteria is the number of iterations. In the first seven additional ANN iterations, the ANN iterates 100 times, the last seven additional ANN iterations took 200 iteration steps.

Despite the additional ANN iteration, the initial ANN parameters $\boldsymbol{w}_1$ must not be too far away from the nominal ANN $\boldsymbol{w}_{nom}$ parameters. We vary the initial ANN parameters by 5, 10 and 15% from the nominal values $\boldsymbol{w}_{nom}$. To do this, we draw 10 times from a normal distribution with the respective n% deviation. The results are presented in Table 4. The RMSE of the non-geometric (NG), geometric (G) and com-

Table 3 Standard deviations of control measures and the observations for scenario a

Std. Dev.	Values
σ_u	0.001°
σ_{tObs}	2.5×10^{-5} m

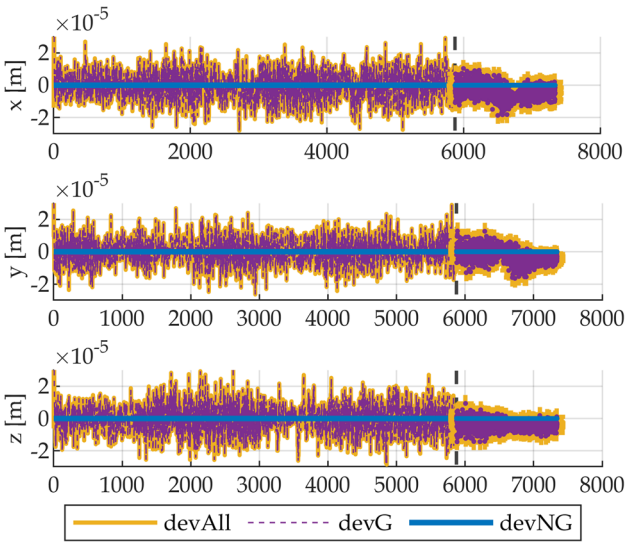

Fig. 9 Result of scenario a. It shows the deviations of the geometric part (devG), the non-geometric part (devNG) and the sum of both parts (devAll). The first 5874 samples were updated in the filter, the following 1468 samples are deviations from the predictions of the test data. The deviations of the geometric and the combined part are in the range of the simulated robot arm position precision

Table 4 Results of deviating nominal ANN parameters by 5, 10 and 15%. The results are mean values out of 10 different ANN parameter initialisations

$\boldsymbol{w}_1$	$\boldsymbol{w}_{nom,5}$	$\boldsymbol{w}_{nom,10}$	$\boldsymbol{w}_{nom,15}$
$RMSE(\boldsymbol{NG})_{test}$	0.18 mm	0.27 mm	0.52 mm
$RMSE(\boldsymbol{G})_{test}$	0.34 mm	0.51 mm	0.69 mm
$RMSE(\boldsymbol{All})_{test}$	0.38 mm	0.53 mm	0.86 mm

bined component (All) is computed for all three scenarios, taking only test data into account. Thus, only the performance in the prediction step is considered. Large non-geometric effects have been simulated (see Fig. 4). Therefore, large RMSE of the single components are achieved. As mentioned in Section 2.2.1, the variation of the whole non-geometric part amounts to 0.6 mm. While considering only the test data of the non-geometric part exhibit a variation of 0.4 mm. Comparing this value with the average test error $RMSE(\boldsymbol{NG})_{test}$, the initial ANN parameters must be better than $\boldsymbol{w}_{nom,15}$ in order to learn the non-geometric part at all. If the initial ANN parameters deviate by 10%, approximately 32.5% of the non-geometric part is learnt. If the initial parameters deviate by only 5%, then 55% of the non-geometric part is determined. It appears to be a very wavy error surface. There is a strong dependence on the initialisation of the ANN parameters to achieve the desired minimum.

Figure 11 and 12 show the results of a realisation with a 5% deviation from $\boldsymbol{w}_{nom}$. Figure 11 shows the deviations of the three components from their nominal values. During filtering (training data), the geometric state and the non-geometric part show the same order of magnitude of deviations with different signs. These are connected by the observation (20). Consequently, the combination of the two components in 'devAll' is almost zero. In the prediction step (test data), the geometric component is constant and

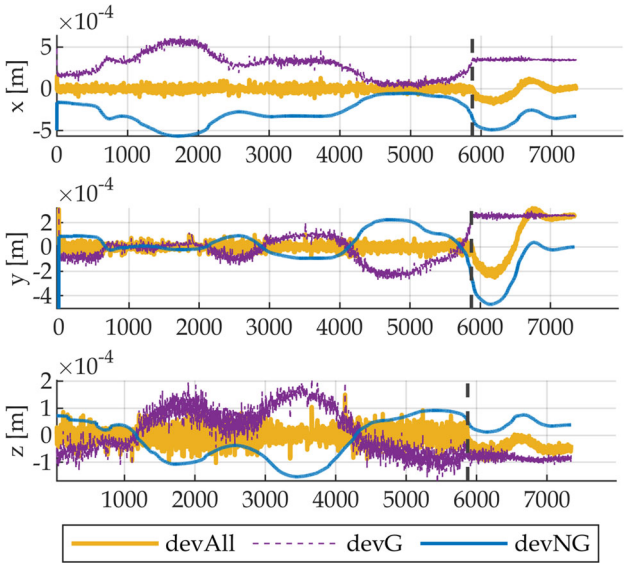

Fig. 11 Result of scenario b inclusive the additional ANN iteration. The initial ANN parameters deviate by 5% of the nominal ones ($\boldsymbol{w}_{nom,5}$). It shows the deviations of the geometric part (devG), the non-geometric (devNG) and the sum of both parts (devAll). The first 5874 samples were updated in the filter, the following 1468 samples are deviations from the predictions of the test data. There are interactions between the geometric state and the non-geometric part

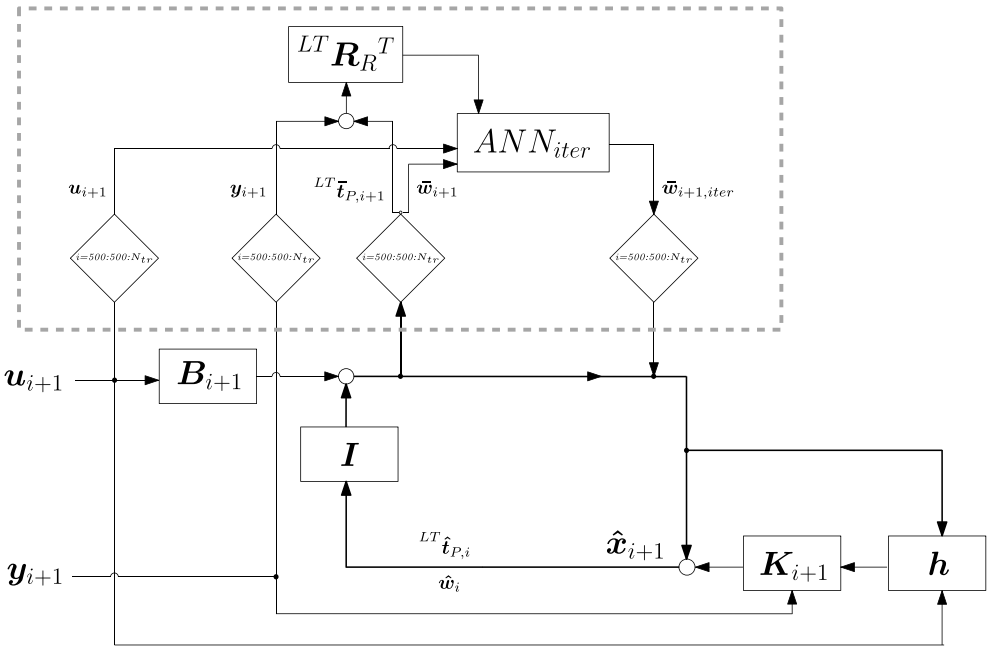

Fig. 10 Additonal iteration of the ANN (ANNiter) after each 500 updated samples up to the number of training samples N_{tr}

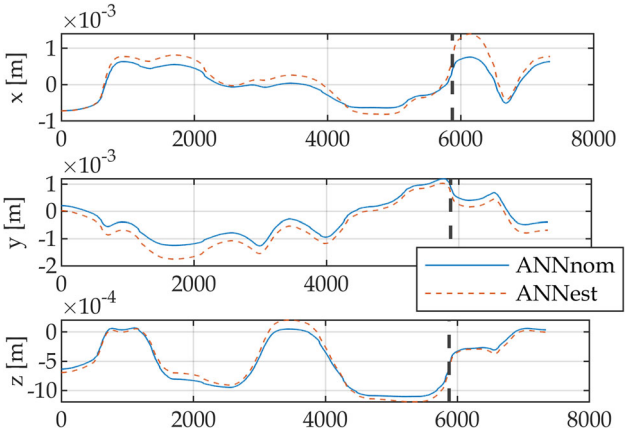

Fig. 12 Result of scenario b inclusive the additional ANN iteration. The initial ANN parameters deviate by 5% of the nominal ones ($\boldsymbol{w}_{nom,5}$). It shows the estimated ANN in comparison to the nominal ANN. The first 5874 samples were updated in the filter, the following 1468 samples are deviations from the predictions of the test data

the level depends on the last filtered state. The prediction of the non-geometric component shows large deviations due to insufficient determination of the ANN. These deviations are visible in Fig. 12 and correspond to the difference between the nominal (ANNnom) and the estimated ANN (ANNest). The predicted combined deviations (devAll, Fig. 11) are mainly driven by the ANN prediction. There is still a need for better ANN determination in the integrated model and a deeper analysis of the interaction between the geometric and the non-geometric part by the stochastic model.

3.3 Sensitivity Analysis

The aim of the sensitivity analysis is to check the influences of the robot arm and transformation parameters, summarised in $\boldsymbol{term}$, on the updated states $\hat{\boldsymbol{x}}$. This is a preliminary step before adaptive filtering in order to show the interactions between the states and the parameters that are to be estimated in the Kalman filter in the future.

The starting point is scenario a. Thus, the ANN parameters are initialised by $\boldsymbol{w}_{nom}$ and the same measurement noise levels are considered (Table 3). We stick to the chosen parameter set in Section 2.2.3. Therefore, only one of the linearly dependent parameters per group is taken into account. Each parameter out of $\boldsymbol{term}$ is biased separately. Metric measures are enlarged by 0.1 mm and angular measures are enlarged by 0.01°.

The resulting deviations of the geometrical translational part $|\boldsymbol{\delta}_G|$ are presented in Fig. 13. There is nearly no effect by the transformation of the robot arm in the laser tracker frame ${}^{LT}\boldsymbol{T}_R$. Due to the relative description in the system equation the transformation ${}^{LT}\boldsymbol{T}_R$ cancels out (14). ${}^{LT}\boldsymbol{R}_R$ only enters in the observation (20). The lever arm component ${}^{RF}\boldsymbol{t}_P$ does not cancel out in Eq. 16. Biases mainly of the x- and y-component have a direct effect on the geometry. The small influence of the z-component ${}^{RF}\boldsymbol{t}_{P,z}$ is due to the specific mounting of the probe. The selected set of $\boldsymbol{dh}_c$ parameters can be estimated. The largest deviations in robot arm geometry are caused by: $d_4, \alpha_4, a_1, a_2, \delta\theta_5$. Small deviations in robot arm geometry may be caused by too little variation in the chosen poses or by a stronger connection to the rotational geometric component.

4 Limitations and Future Work

The overall aim of integrating the parametric and non-parametric approach is to achieve an unbiased estimate of the robot arm system by taking all influencing variables into account. The approach presented has some shortcomings or limitations at the present time, which are summarised in the following.

The developed method is based on 6DOF laser tracker measurements on a probe mounted on the robot arm flange. Therefore, the pose of the probe in the laser tracker system ${}^{LT}\boldsymbol{T}_{P,i}$ is contained in the method and represents the 'true' robot arm pose.

At the present time, only the lever arm ${}^{RF}\boldsymbol{t}_P$ between probe and robot flange is considered in the algorithm. The orientation component ${}^{RF}\boldsymbol{R}_P$ is neglected due to the parallel mounting of the probe frame in dependence to the robot flange frame (${}^{RF}\boldsymbol{R}_P = \boldsymbol{I}$).

As required by the first basic concept, all parameters that will be estimated adaptively in the future should be included in the system description. The system (14) does not include ${}^{LT}\boldsymbol{T}_R$. The sensitivity analysis (Sec. 3.3) confirms this statement. However, the transformation ${}^{LT}\boldsymbol{T}_R$ is mainly of interest for comparison with the PCM or with other calibration methods. The main focus is on the robot arm parameter $\boldsymbol{dh}$ and these can be estimated (see Section 3.3).

At this stage of development of the approach it is particularly important to have good initial values for the various parameters. The most critical group are the ANN parameters. We have shown in Section 3.2 that we need ANN parameters that are better than 15% for this particular simulation setup in order to estimate ANN parameters in a meaningful way. This is even more relevant in view of measured data. Initial values of the transformation parameters can be calculated from the PCM. The $\boldsymbol{dh}$ parameters of the robot arm can be initialised by the values used by the robot arm. The ANN parameters are problematic because they differ greatly from those in the PCM due to the sequential determination of the robot's position corrections. An iterative determination of the PCM could provide better initial values.

In order to achieve the full functionality of the proposed integrated approach, some steps still need to be

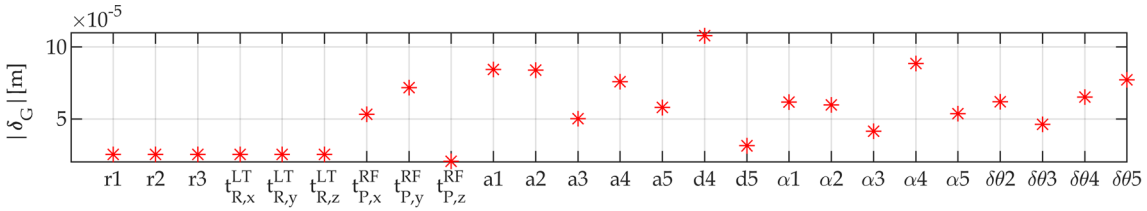

Fig. 13 Result of the sensitivity analysis for the geometrical part (G) in dependence of variations in $\boldsymbol{term}$

taken. First of all, the interactions between the geometric and non-geometric part must be checked. Second, the robot parameters $\boldsymbol{dh}_c$ inclusive the transformation parameters ${}^{LT}\boldsymbol{T}_R$, ${}^{RF}\boldsymbol{t}_P$ are to be estimated adaptively in the filter.

The ANN iteration according to scenario b (Sec. 3.2) is applied in addition to the adaptive filtering. Thereby the full functionality of the approach is achieved. At present, it is not yet possible to predict how the determination of the transformation and robot parameters will affect the estimation of the ANN parameters and vice versa. Therefore, an important instrument for controlling this interaction in future is the stochastic model used in the EKF.

The fourth important step is the validation of the integrated approach on real data when the full functionality of the approach is achieved. A comparison with the PCM and other robot calibration approaches is mandatory. In that step, a procedure to reach appropriate initial values for the ANN parameters needs to be developed.

5 Conclusion

We introduce a framework to integrate the geometric robot arm model with the non-geometric one realised by an ANN. In this way, we are pursuing the goal of an unbiased description of the robot arm system and thus achieve a more accurate position description. The simultaneous estimation of geometric and non-geometric error sources by a combination of parametric and non-parametric approaches has not yet been topic of robot arm calibration research. The usual approach is to first model parametrically and in a second sequential step to describe the residuals using non-parametric approaches (model-observation mismatch approach).

In a preliminary study (Sec. 2.2.2), we show that a sequential procedure can lead to biased estimates. The calculation of transformation parameters in a transformation procedure and in the course of kinematic calibration (Sec. 2.2) are compared. Only the estimation of the transformation parameters in the extended approach leads to a more unbiased estimation of the transformation and lever arm parameters. The similarity of the "absorbed" parameters in the transformation and lever arm determination with the linearly dependent parameters in the kinematic robot calibration is recognisable. An extension with the dynamic modelling of the robot arm is necessary due to a too large model-observation mismatch. This was shown in preliminary work on kinematic calibration (see Section 2.2.3, [35]). As the literature ([10], [25]) shows, the use of ML is a suitable tool for modelling dynamic effects. All these findings lead to the formulation of the simultaneous estimation of the geometric and non-geometric parameters of the robot arm.

The EKF offers the option of adding a geometric/physical model to the system description. The ANN is placed in the observation equation. The combination of both components takes place in the observation equation. There, the predicted state (geometric part) and the transformed ANN (non-geometric part) add up to the observation. The functionality is verified using simulated data. The adjustment of the non-geometric part by the ANN is not achieved by randomised initial ANN parameters. ANN adaptation based on one data sample under slightly different conditions per update step is not sufficient. For this reason, we pursue the idea of an additional ANN iteration. The additional ANN iteration is considered in the prediction step. This shows that the initial ANN parameters must not deviate too much. Otherwise, no convergence is achieved. If the initial ANN parameters deviate by 10% from the target values, around 32.5% of the non-geometric component is learnt.

The developed integrated approach enables a separation between the 'knowledge-strong' (physical/geometrical model) and the 'knowledge weak or very complex' (non-parametric model) parts [11]. This differentiation achieves a certain degree of interpretability and is therefore considered to be another important advantage of the developed approach in addition to the unbiased estimation.

Author Contributions Both authors contributed to the study conception and design. Material preparation, data simulation and analysis were performed by Sabine Horvath. The first draft of the manuscript was written by Sabine Horvath and both authors commented on previous versions of the manuscript. Both authors read and approved the final manuscript.

Funding Open access funding provided by TU Wien (TUW). The authors acknowledge TU Wien Bibliothek for financial support through its Open Access Funding Program.

Declarations

Ethics Approval Not Applicable.

Consent for Publication Not Applicable.

Consent for Participate Not Applicable.

Conflict of Interest Not Applicable.

References

1. Liu, N., Zhang, X., Zhang, L., Shang, D., Fan, X.: Study on the Rigid-Flexible Coupling Dynamics of Welding Robot. Wirel. Pers. Commun. **102**(2), 1683–1694 (2018). https://doi.org/10.1007/s11277-017-5227-7. Accessed 2024-06-17
2. Jiang, D., Li, G., Sun, Y., Hu, J., Yun, J., Liu, Y.: Manipulator grabbing position detection with information fusion of color image and depth image using deep learning. J. Ambient. Intell. Humaniz. Comput. **12**(12), 10809–10822 (2021). https://doi.org/10.1007/s12652-020-02843-w. Accessed 2024-06-17
3. Li, X.: Robot target localization and interactive multi-mode motion trajectory tracking based on adaptive iterative learning. J. Ambient. Intell. Humaniz. Comput. **11**(12), 6271–6282 (2020). https://doi.org/10.1007/s12652-020-01878-3. Accessed 2024-06-19
4. Parikh, P., Trivedi, R., Dave, J., Joshi, K., Adhyaru, D.: Design and development of a low-cost vision-based 6 DoF assistive feeding robot for the aged and specially-abled people. IETE J. Res. **70**(2), 1716–1744 (2024). https://doi.org/10.1080/03772063.2023.2173665. Accessed 2024-06-17
5. Schmidt, R.M., Schitter, G., Eijk, J.v.: The Design of High Performance Mechatronics: High-tech Functionality by Multidisciplinary System Integration, Third revised edition edn. Delft University Press, Amsterdam (2020). OCLC: 1145888837
6. Siciliano, B., Khatib, O. (eds.): Springer Handbook of Robotics: with ... 84 Tables. Springer, Berlin (2008). OCLC: 244008134
7. El Hamidi, K., Mjahed, M., El Kari, A., Ayad, H., El Gmili, N.: Design of hybrid neural controller for nonlinear MIMO system based on NARMA-L2 model. IETE J. Res. **69**(5), 3038–3051 (2023). https://doi.org/10.1080/03772063.2021.1909507. Accessed 2024-06-19
8. Hastie, T., Tibshirani, R., Friedman, J.H.: The Elements of Statistical Learning: Data Mining, Inference, and Prediction, Second edition, corrected at 12th printing 2017 edn. Springer series in statistics. Springer, New York, NY (2017). https://doi.org/10.1007/b94608
9. Wu, Y., Klimchik, A., Caro, S., Furet, B., Pashkevich, A.: Geometric calibration of industrial robots using enhanced partial pose measurements and design of experiments. Robot. Comput.-Integr. Manuf. **35**, 151–168 (2015). https://doi.org/10.1016/j.rcim.2015.03.007. Accessed 2017-03-22
10. Aoyagi, S., Kohama, A., Nakata, Y., Hayano, Y., Suzuki, M.: Improvement of robot accuracy by calibrating kinematic model using a laser tracking system-compensation of non-geometric errors using neural networks and selection of optimal measuring points using genetic algorithm-. In: 2010 IEEE/RSJ International Conference on Intelligent Robots and Systems, pp. 5660–5665. IEEE, Taipei (2010). https://doi.org/10.1109/IROS.2010.5652953. http://ieeexplore.ieee.org/document/5652953/ Accessed 2024-03-26
11. Reichstein, M., Camps-Valls, G., Stevens, B., Jung, M., Denzler, J., Carvalhais, N.: Prabhat: deep learning and process understanding for data-driven Earth system science. Nature **566**(7743), 195–204 (2019). https://doi.org/10.1038/s41586-019-0912-1. Accessed 2024-03-26
12. Shlezinger, N., Whang, J., Eldar, Y.C., Dimakis, A.G.: Model-based deep learning. Proc. IEEE **111**(5), 465–499 (2023). https://doi.org/10.1109/JPROC.2023.3247480. Accessed 2024-03-26
13. Jin, X.-B., Robert Jeremiah, R.J., Su, T.-L., Bai, Y.-T., Kong, J.-L.: The New Trend of State Estimation: From Model-Driven to Hybrid-Driven Methods. Sensors. **21**(6), 2085 (2021). https://doi.org/10.3390/s21062085. Accessed 2024-03-26
14. Bai, Y., Yan, B., Zhou, C., Su, T., Jin, X.: State of art on state estimation: Kalman filter driven by machine learning. Annu. Rev. Control. **56**, 100909 (2023). https://doi.org/10.1016/j.arcontrol.2023.100909. Accessed 2024-03-26
15. Nguyen, H.-N., Zhou, J., Kang, H.-J.: A calibration method for enhancing robot accuracy through integration of an extended Kalman filter algorithm and an artificial neural network. Neurocomputing **151**, 996–1005 (2015). https://doi.org/10.1016/j.neucom.2014.03.085. Accessed 2018-07-19
16. Stubberud, S.C., Lobbia, R.N., Owen, M.: An adaptive extended Kalman filter using artificial neural networks. In: Proceedings of 1995 34th IEEE Conference on Decision and Control, vol. 2, pp. 1852–1856. IEEE, New Orleans, LA, USA (1995). https://doi.org/10.1109/CDC.1995.480611. http://ieeexplore.ieee.org/document/480611/ Accessed 2024-03-26
17. Haykin, S.S.: Kalman Filtering and Neural Networks. Wiley, New York (2001). http://search.ebscohost.com/login.aspx?direct=true&scope=site&db=nlebk&db=nlabk&AN=82009 Accessed 2015-11-07
18. Abbeel, P., Coates, A., Montemerlo, M., Y. Ng, A., Thrun, S.: Discriminative training of Kalman Filters. In: Robotics: Science and Systems I. Robotics: Science and Systems Foundation, Cambridge, Massachusetts (2005). https://doi.org/10.15607/RSS.2005.I.038. http://www.roboticsproceedings.org/rss01/p38.pdf Accessed 2024-03-26
19. Xu, L., Niu, R.: EKFNet: Learning system noise statistics from measurement data. In: ICASSP 2021 - 2021 IEEE International Conference on Acoustics, Speech and Signal Processing (ICASSP), pp. 4560–4564. IEEE, Toronto, ON, Canada (2021). https://doi.org/10.1109/ICASSP39728.2021.9415083. https://ieeexplore.ieee.org/document/9415083/ Accessed 2024-03-26
20. Daw, A., Karpatne, A., Watkins, W., Read, J., Kumar, V.: Physics-guided neural networks (PGNN): an Application in Lake Temperature Modeling. arXiv. arXiv:1710.11431 [physics, stat] (2021). http://arxiv.org/abs/1710.11431 Accessed 2024-03-26
21. Willis, M.J., Von Stosch, M.: Simultaneous parameter identification and discrimination of the nonparametric structure of hybrid semi-parametric models. Comput. Chem. Eng. **104**, 366–

376 (2017). https://doi.org/10.1016/j.compchemeng.2017.05.005. Accessed2024-03-26
22. Fan, M., Bai, Y., Wang, L., Ding, L.: Combining a fully connected neural network with an ensemble Kalman filter to emulate a dynamic model in data assimilation. IEEE Access. **9**, 144952–144964 (2021). https://doi.org/10.1109/ACCESS.2021.3120482. Accessed 2024-03-26
23. Revach, G., Shlezinger, N., Ni, X., Escoriza, A.L., Sloun, R.J.G., Eldar, Y.C.: KalmanNet: Neural Network Aided Kalman Filtering for Partially Known Dynamics. IEEE Transactions on Signal Processing. **70**, 1532–1547 (2022) https://doi.org/10.1109/TSP.2022.3158588 . arXiv:2107.10043 [cs, eess, stat]. Accessed 2024-03-26
24. Zhao, G., Zhang, P., Ma, G., Xiao, W.: System identification of the nonlinear residual errors of an industrial robot using massive measurements. Robot. Comput. Integr. Manuf. **59**, 104–114 (2019). https://doi.org/10.1016/j.rcim.2019.03.007. Accessed 2024-03-26
25. Gadringer, S., Gattringer, H., Müller, A., Naderer, R.: Robot calibration combining kinematic model and neural network for enhanced positioning and orientation accuracy. IFAC-PapersOnLine. **53**(2), 8432–8437 (2020). https://doi.org/10.1016/j.ifacol.2020.12.1436. Accessed 2024-03-26
26. Selingue, M., Olabi, A., Thiery, S., Béarée, R.: Hybrid calibration of industrial robot considering payload variation. J. Intell. Robot. Syst. **109**(3), 58 (2023). https://doi.org/10.1007/s10846-023-01980-6. Accessed 2024-03-27
27. Horvath, S., Neuner, H.: System identification of a robot arm with extended Kalman filter and artificial neural networks.pdf. Journal of Applied Geodesy. **13**(2), 135–150
28. Ali, I., Suominen, O., Gotchev, A., Morales, E.R.: Methods for Simultaneous Robot-World-Hand-Eye Calibration: a Comparative Study. Sensors. **19**(12), 2837 (2019). https://doi.org/10.3390/s19122837. Accessed 2024-03-26
29. Denavit, J., Hartenberg, R.S.: A Kinematic notation for lower-pair mechanisms based on matrices. J. Appl. Mech. **22**(2), 215–221 (1955). https://doi.org/10.1115/1.4011045. Accessed 2024-03-27
30. Mooring, B., Roth, Z., Driels, M.: Fundamentals of Manipulator Calibration. John Wiley & Sons, New York (1991)
31. Bishop, C.M.: Pattern Recognition and Machine Learning. Information science and statistics. Springer, New York (2006)
32. Haykin, S.S.: Neural Networks - A Comprehensive Foundation, 2nd, edition Prentice Hall, NJ (1999)
33. Gelb, A.: Applied Optimal Estimation. Mass. Institute of Technology, Cambridge, MA, Cambridge (1974)
34. Singhal, S., Wu, L.: Training multilayer perceptrons with the extended Kalman algorithm. In: Advances in Neural Information Processing Systems, pp. 133–140 (1989)
35. Pühringer, M.: Beiträge zur kinematischen und dynamischen Kalibrierung eines Industrie-Roboterarmes. Master's thesis, TU Wien, Vienna (2019)
36. Ghilani, C.D., Wolf, P.R.: Adjustment Computations: Spatial Data Analysis, 1st edn. Wiley, Hoboken, NJ (2006). https://doi.org/10.1002/9780470121498. https://onlinelibrary.wiley.com/doi/book/10.1002/9780470121498 Accessed 2024-03-27
37. Montavon, G., Orr, G.B., Müller, K.-R.: Neural Networks: Tricks of the Trade, 2nd ed edn. Lecture notes in computer science, vol. 7700. Springer, Berlin New York (2012)

Sabine Horvath is a research assistant at the Department of Geodesy and Geoinformation, TU Wien. She received her MSc degree in 2014 and her research focuses on the use of artificial neural networks for modelling robotic arms or real estate valuation.

Hans Neuner is Prof. for Engineering Geodesy at the Department of Geodesy and Geoinformation, TU Wien. He received his doctoral degree from Leibniz Universität Hannover in 2007. His research focuses on geodetic deformation analysis, deformation measurements, terrestrial laser scanning, kinematic measurement methods, filter methods in state space and industrial surveying.